Nucleation and early seismic propagation of small and large events in a crustal earthquake model

Nadia Lapusta[1]

Division of Engineering and Applied Sciences, Harvard University, Cambridge, Massachusetts, USA

James R. Rice

Department of Earth and Planetary Sciences and Division of Engineering and Applied Sciences, Harvard University, Cambridge, Massachusetts, USA

Received 10 July 2001; revised 11 July 2002; accepted 6 January 2003; published 18 April 2003.

[1] Earthquake nucleation and early seismic propagation are studied in a two-dimensional strike-slip fault model with depth-variable properties. The fault is governed by the Dieterich-Ruina rate and state friction law. We use an efficient and rigorous numerical procedure for elastodynamic analysis of earthquake sequences on slowly loaded faults developed by *Lapusta et al.* [2000]. We find that for decreasing values of the characteristic slip distance of the friction law, small events appear at the transition from the locked to creeping behavior toward the bottom of the seismogenic zone. Small and large events have very similar nucleation phases in our simulations. Here, by "nucleation phase" we mean gradually accelerating aseismic slip in a small slowly expanding zone before the breakout of the dynamic, seismically detectable event. Moment acceleration (to which velocity seismograms are proportional) in early stages of seismic propagation exhibits irregular fluctuations, in the form of speedups and slowdowns in the moment release rate, consistently with observations as reported by *Ellsworth and Beroza* [1995]. Our simulations show that such irregular moment acceleration can, at least in part, be due to the heterogeneous stress distribution imprinted on the fault by the arrest of previous small events and by stress concentrations at the borders of creeping regions and to partial arrest of the rupture in velocity-strengthening fault regions which inhibit seismic slip. *INDEX TERMS:* 7209 Seismology: Earthquake dynamics and mechanics; 7260 Seismology: Theory and modeling; 3220 Mathematical Geophysics: Nonlinear dynamics; 7230 Seismology: Seismicity and seismotectonics; 3230 Mathematical Geophysics: Numerical solutions; 8164 Tectonophysics: Stresses—crust and lithosphere; *KEYWORDS:* earthquake nucleation phase, event clustering, irregular moment release, stress concentrations, rate and state friction, earthquake sequences

Citation: Lapusta, N., and J. R. Rice, Nucleation and early seismic propagation of small and large events in a crustal earthquake model, *J. Geophys. Res.*, *108*(B4), 2205, doi:10.1029/2001JB000793, 2003

1. Introduction

[2] Understanding the development and initial stages of an earthquake rupture is a major goal of earthquake science. The purpose of this work is to identify the factors controlling the nucleation and early seismic propagation of simulated earthquakes, which are part of a sequence of dynamic events predicted by analysis of a two-dimensional (2-D) depth-variable crustal earthquake model. That model is subjected to slow tectonic loading, incorporates laboratory-derived rate and state friction laws with realistic parameters, and includes full account of inertial effects. These are simulations of the type initiated by *Tse and Rice* [1986], updated [*Rice*, 1993] with inclusion of data on granite gouge under hydrothermal conditions [*Blanpied et al.*, 1991, 1995], put in the context of fully inertial elastodynamics [*Rice and Ben-Zion*, 1996; *Ben-Zion and Rice*, 1997], and embedded within highly efficient computational algorithms [*Lapusta et al.*, 2000].

[3] The study was prompted by the appearance of small events in our simulations [*Lapusta et al.*, 2000] as we decrease the characteristic slip distance L for state evolution (renewal of asperity contact population) in rate and state friction laws. This gives us the opportunity to compare the nucleation of large and small events in our simulations and to study what we find to be the important effects of prior small events on the early seismic phases of large events. The small events appear in the vicinity of the deep transition between the locked and the creeping regions (i.e., the transition from velocity-weakening to velocity-strengthening behavior at depth, where temperatures are approximately 300°C). Clustering of small events at such transitions is not unexpected,

[1]Now at Division of Engineering and Applied Science and Division of Geological and Planetary Sciences, California Institute of Technology, Pasadena, California, USA.

0148-0227/03/2001JB000793$09.00

since it is there that creeping regions cause stress concentration. Such clustering is observed on real faults, as we show from results of others based on precise events relocations for the Parkfield region [*Ellsworth et al.*, 2000] of the San Andreas fault and the Calaveras fault [*Schaff et al.*, 2002].

[4] The problem of earthquake nucleation currently enjoys a lot of interest, because of its fundamental importance for the physics of earthquakes as well as because of the immediate practical implications. A major question is whether the nucleation process and the ultimate size of the resulting earthquake are related or not. If they are, then we could predict the size of an earthquake by its nucleation process, if we are able to detect it (and could make effective use of that detection to provide short-term warnings). Some researchers suggest, or at least present supporting evidence, that the nucleation process, specifically the size of the nucleation zone, is indeed related to the ultimate size of the resulting earthquake, in that the larger the earthquake, the larger its nucleation zone [e.g., *Ohnaka*, 1993; *Ellsworth and Beroza*, 1995; *Dodge et al.*, 1996]. Others support the view that the nucleation size is unrelated to the final size of an earthquake [e.g., *Abercrombie and Mori*, 1994; *Mori and Kanamori*, 1996; *Kilb and Gomberg*, 1999]. In our modeling, the nucleation process, in the sense of transition from initially aseismic slippage at an accelerating rate to the onset of a dynamic break out, is virtually identical for large and small events, as we demonstrate in section 3.3. Hence our modeling supports the view that large earthquakes are small earthquakes that run away due to favorable conditions on the fault.

[5] We also study in detail dynamic rupture propagation of large events. This is motivated by the results of *Ellsworth and Beroza* [1995], who show that the initial velocity seismograms in many real earthquakes are somewhat intermittent, with speedups and slowdowns before onset of an often much greater speedup associated with the primary moment release. *Ellsworth and Beroza* [1995] attributed that initial reluctant phase to the propagation of ruptures over either their nucleation zones or a special cascade-like structure of the fault. In our simulations, large events exhibit slowdowns and speedups in moment acceleration during their propagation outside of their nucleation zone. As we will show, the most notable irregularities we observe are caused by either stress concentration left by arrest of previous small events or by partial arrest of the rupture in the velocity-strengthening (and hence slip-inhibiting) region. Stress concentration at the ends of creeping regions also affects moment acceleration. We therefore suggest that an important route to understanding the early moment release, or what might be called the ''seismic nucleation phase,'' will be to understand what controls stress patterns where events nucleate.

[6] The challenge of simulating earthquake sequences, with emphasis on both careful resolution of aseismic and nucleation processes and incorporation of all dynamic effects, becomes very clear if we consider the variety of temporal and spatial scales we have to deal with. Let us consider the spatial scales first. One has to simulate a fault region which is at least tens to hundreds of kilometers, while resolving properly slip in nucleation zones and at the tips of propagating ruptures. The size of a nucleation zone is proportional to the characteristic slip distance L for evolution of interface state (a parameter in laboratory-derived rate and state friction laws we use), with the factor being a few times 10^5 for the physical parameters of our model. Hence the nucleation size would be a few meters for $L = 10$ μm. Since grid size must be much smaller than that, such values are hardly tractable numerically. Thus one has to use larger values of L in simulations, and part of this study is directed toward establishing the effects of using more realistic values of L. Moreover, the zones of very rapid stress and state evolution at rupture fronts also scale with L, being still much smaller than the nucleation size and hence more demanding computationally. For example, with $L = 2$ mm (which is too large), we establish from our simulations that the nucleation zone is $\sim$0.8 km, whereas the zone of rapid accumulation of slip at the rupture front is of order 0.06 km, which is more than 10 times smaller. So we see that the spatial scales in this problem vary from tens of kilometers to fractions of a meter (if to deal with L in the laboratory range).

[7] Let us consider now the temporal scales. The typical tectonic loading rate, measured in terms of plate velocities, is of the order of tens of millimeters per year. A typical large earthquake accumulates meters of slip in one event. Hence, to produce a sequence of events, we should be able to simulate thousands of years of loading, accounting for stress redistribution due to aseismic slipping (creep) on some parts of the fault and modeling accurately the nucleation of unstable slip (model earthquake), which is a very gradual process. On the other hand, a dynamic event, when it occurs, is over in tens to hundreds of seconds (as characterized by the time for elastic waves to transverse the fault segment of interest). In addition, slip velocities during unstable slip are of the order of a meter per second, and are presumably much higher at the tips of propagating rupture fronts. To resolve these (high) slip velocities (which also depend on L, being larger for smaller L), very fine stepping in time (associated with the fine discretization in space discussed) is required. Hence we have at least three different timescales: the loading timescale of the order of hundreds of years, the event timescale of the order of tens of seconds, and the timescale of numerical resolution of the order of small fractions of a second. Adding to this the necessity to account for inertial effects, we get a very complex and challenging problem.

[8] To overcome the problem of combining these multiple timescales, several approaches were developed: To load the model instantaneously to a level for which the instability starts at once, at the expense of neglecting all aseismic slip; To model aseismic deformation using a quasi-static method, switching to a dynamic method during instability; To impose such a high plate rate (many orders of magnitude higher than on real faults) that a standard dynamic method can be used on all stages of the simulation [*Lapusta et al.*, 2000, and references therein]. All these approaches can potentially disrupt the development of the model earthquake and/or its initial dynamic propagation.

[9] We use the methodology developed by *Lapusta et al.* [2000], which is ideally suited for the study of processes before, during, and after the nucleation of a model earthquake, since it fully resolves all stages of an earthquake episode, preventing the potential disruption of the simulated process of earthquake development. The method allows us to simulate quasi-static deformation on the creeping (velocity-strengthening) parts of the fault that proceeds at millimeters per year, the nucleation process of gradually accelerating aseismic slip in a small slowly expanding zone, the follow-

ing dynamic, inertially controlled event, with slip velocities of order of meters per second and rupture velocities of order of kilometers per seconds, and resulting postseismic slip.

2. Methodology and Problem Formulation

[10] The methodology and problem formulation are described in detail by *Lapusta et al.* [2000]. We summarize the important points below.

2.1. Methodology: Two Main Ingredients

[11] One of the main difficulty in modeling earthquake sequences is the necessity to combine long simulation times with the resolution of inertial (or dynamic) effects. Our methodology uses a spectral representation of the boundary integral formulation [*Lapusta et al.*, 2000, and references therein], in which the computationally intensive part of inertial effects is represented by time convolution integrals on Fourier components of deformation (slip velocity). These convolutions have rapidly decaying kernels, reflecting the fact that long prior deformation history has negligible contribution. Hence to treat the dynamic effects accurately, we need to account for the influence of recent deformation only and can truncate the convolution integrals. Such truncation is the first important ingredient of our methodology.

[12] The second ingredient, variable time stepping, allows us to get through periods of quasi-static deformation, when things happen very slowly, in relatively few large time steps (of order of a fraction of a year), while studying carefully the nucleation and dynamic propagation of model earthquakes by gradually decreasing time steps until they reach a small fraction of a second. To accomplish that, we essentially take the time step to be inversely proportional to slip velocity. The coefficients of proportionality depend on the parameters of the constitutive law and the space discretization. They were derived based on physical considerations and numerical stability requirements for a general class of rate and state friction laws with a positive direct velocity effect [*Lapusta et al.*, 2000]. We note that the developed stepping scheme enables taking large time steps during quasi-static periods without losing stability only for constitutive laws with nonzero direct velocity effect. Hence the scheme is not directly applicable to laws without that effect, such as slip-weakening laws.

2.2. The 2-D Depth-Variable Model With Rate and State Friction

[13] We apply the procedure to a 2-D vertical strike-slip fault in which slip is constrained to vary with depth only (there is no variation along strike) (Figure 1). The fault is loaded with the equivalent of plate velocity of 35 mm/yr. We model the free surface effects using a mirror image. The problem can be expressed in the 2-D antiplane framework.

[14] The constitutive law used is based on the Dieterich-Ruina (logarithmic) rate and state friction, which has the form

$$\tau(z,t) = \bar{\sigma}(z)\left[f_o + a(z)\ln\frac{V(z,t)}{V_o} + b(z)\ln\frac{V_o\theta(z,t)}{L(z)}\right], \quad (1a)$$

$$\frac{\partial\theta(z,t)}{\partial t} = 1 - \frac{V(z,t)\theta(z,t)}{L(z)}. \quad (1b)$$

Here t, τ, $\bar{\sigma}$, V, and θ are the time, frictional stress, effective normal stress, slip velocity, and state variable, respectively; $f_o = 0.6$ is the value of friction coefficient at the reference velocity $V_o = 1$ μm/s; a and b are frictional parameters; and L is the characteristic slip distance for evolution of frictional strength. The characteristic slip distance L is the sliding distance for renewal of the population of asperity contacts [*Dieterich and Kilgore*, 1994, 1996].

[15] Note that this law incorporates only logarithmic rate weakening at high slip rates, whereas there is some experimental evidence that stronger weakening may take place at high slip rates [*Lim et al.*, 1989; *Tsutsumi and Shimamoto*, 1997]. This stronger weakening is thought to be due to thermal softening, initially by flash heating at asperity contacts and, at more severe conditions, by local melting [e.g., *Lim and Ashby*, 1987; *Molinari et al.*, 1999; *Rice*, 1999]. Inclusion of the stronger weakening would not directly modify the nucleation and early rupture propagation, which are the main objects of this study. However, further rupture propagation would certainly be affected, which in turn can affect the mode, overall slip, and arrest of ruptures, and hence the earthquake sequence as a whole. That is why it is important to include stronger weakening at high slip rates (and/or slips) in future studies.

[16] The experimental and physical basis for this type of laws, their formulation, stability properties, necessity to avoid the ill-posedness of some simpler friction models, and choice of parameters are discussed by *Lapusta et al.* [2000], *Rice et al.* [2001], and *Lapusta* [2001] and references therein. We regularize the law (1) near $V = 0$, in a manner consistent with a thermally activated creep model of the direct effect, and allow V of either sign, to get

$$\tau = a\,\bar{\sigma}\,\mathrm{arcsinh}\left[\frac{V}{2V_o}\exp\left(\frac{f_o + b\ln(V_o\theta/L)}{a}\right)\right], \quad (2a)$$

$$\frac{\partial\theta(z,t)}{\partial t} = 1 - \frac{|V(z,t)|\theta(z,t)}{L(z)}. \quad (2b)$$

[17] The depth-variable frictional properties of the fault are demonstrated in Figure 2. The fault exhibits steady state velocity-strengthening friction right next to the free surface and at the bottom, while the region in between has steady state velocity-weakening properties and hence can produce model earthquakes. For all cases studied here and by *Lapusta et al.* [2000], the effective normal stress incorporates high fluid over pressurization at depth, so that $\bar{\sigma} = \min$ [2.8 + (18 z/km), 50] MPa [*Rice*, 1992, 1993]. Hence $\bar{\sigma}$ is relatively small at depth (50 MPa). This makes simulations more tractable for given L, $b - a$, and a but also reduces the size of earthquake slips and stress drops in the deeper parts of the fault comparing to the case with no high fluid over pressurization at depth in which $\bar{\sigma}$ would keep increasing linearly with depth. Note that $\bar{\sigma}$ is constant in time in this study. Our methodology allows to consider $\bar{\sigma}$ variable in time, for example, due to pore pressure evolution in response to shear heating effects. However, in the case of variable normal stress, the framework (1) has to be modified, to include memory effects with respect to temporal variations in normal stress [*Rice et al.*, 2001, and references therein].

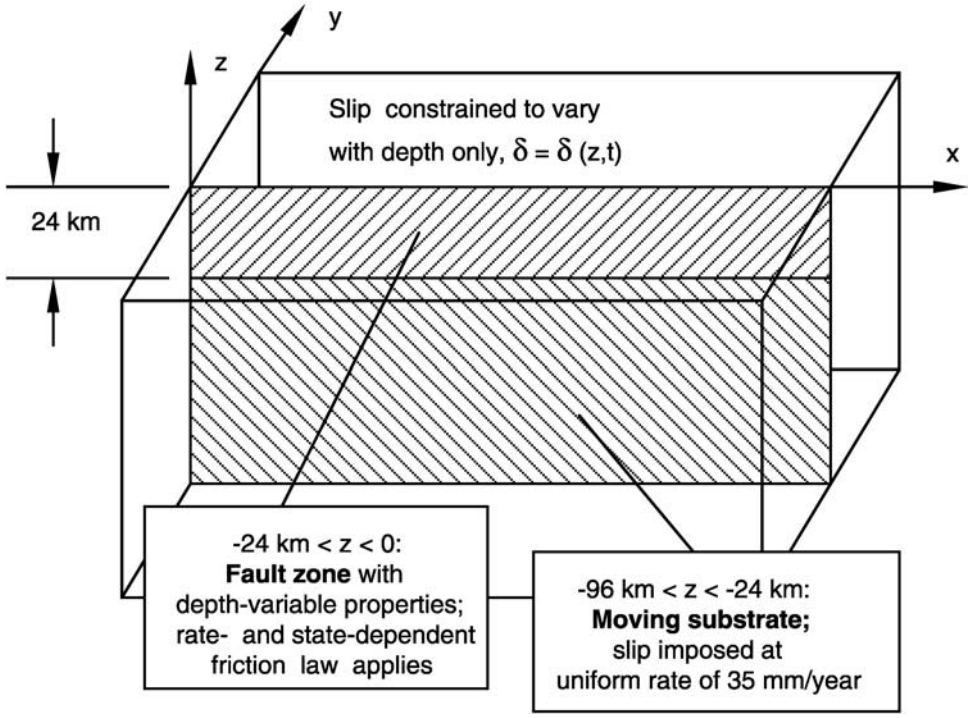

Figure 1. A vertical strike-slip fault in an elastic half-space (as used by *Lapusta et al.* [2000] and earlier studies).

[18] The distribution of frictional properties (in particular, of the characteristic slip distance L) and normal stress is fixed throughout the seismogenic (velocity-weakening) part of the fault. Hence there are no imposed heterogeneities within the seismogenic part. This is, obviously, a simplification, which we adopt to find the qualitative effects of combining slow loading, rate and state friction, and inertia, with no interference from the potential effects of heterogeneities, other than those required by the variation with depth of temperature-dependent properties. The absence of smaller-scale heterogeneities also makes the problem more tractable numerically. Inclusion of such

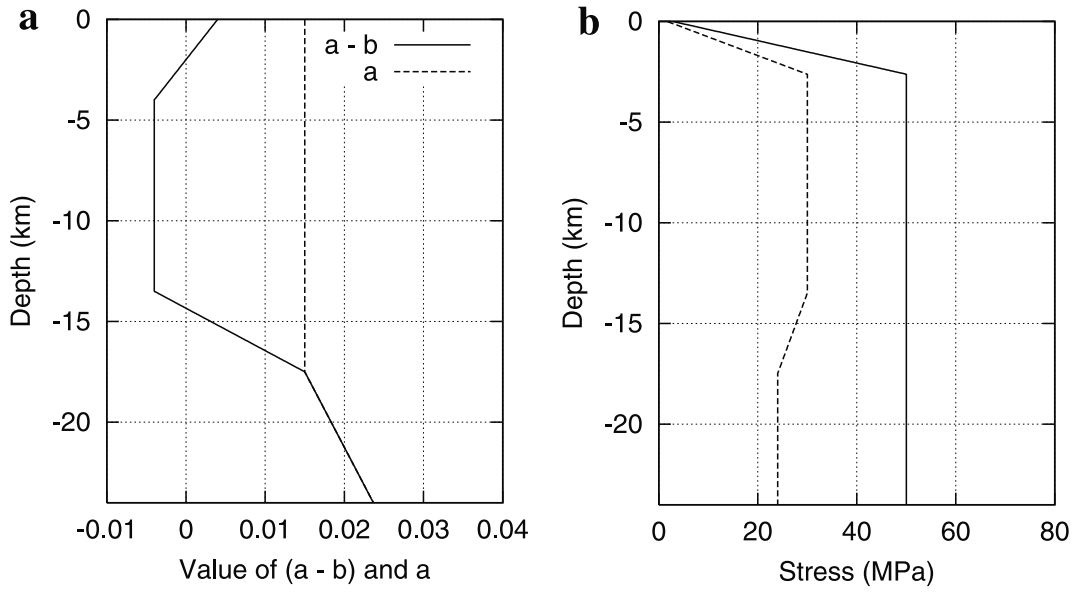

Figure 2. (a) Depth-variable distribution of frictional parameters ($a - b$) and a, the former from *Blanpied et al.* [1991, 1995] as adapted by *Rice* [1993] for granite gouge under hydrothermal conditions. (b) Depth-variable distribution of the effective normal stress $\bar{\sigma}$ (solid line) and initial shear stress $\tau^o(z)$ (dashed line). From *Lapusta et al.* [2000].

heterogeneities can be an important next step, but it is not pursued in this study.

2.3. On the Characteristic Slip Distance of Rate and State Friction

[19] The rate and state friction formulation (1) incorporates characteristic slip distance L (sometimes also called D_c or d_c). Distance L represents the characteristic slip required for evolution of the state variable θ to its steady value following the perturbation in slip velocity. The experimentally derived values of L are of order 1 to 100 μm. They are too small to be tractable numerically even in 2-D simulations of the type considered here, to say nothing of 3-D ones. That is why much larger values of L, of order of millimeters to tens of millimeters, are typically used in simulations. Such compromises are common for many areas of computational physics with similar limitations stemming from smallness of physical parameters (e.g., viscosity in common fluids). A viable approach, in those circumstances, is to choose L so as to make the nucleation size small compared to other length scales in the problem (e.g., as set by gradients with depth in friction properties), and then to study how the response of the model changes as we decrease L, approaching the laboratory range. This is the approach taken in the following sections.

[20] There is much debate whether the laboratory-derived values of characteristic slip distance L are applicable to real faults. We believe that they are, for the following reason. It is possible to estimate the values of L on faults from the smallest earthquakes that occur. The size of these smallest earthquakes, of the order 1 m, should be comparable to the size h_{nucl} of the smallest zone that can produce unstable slip. From stability studies [e.g., *Rice and Ruina*, 1983; *Rice et al.*, 2001], h_{nucl} scales with L, being approximately proportional to L, but multiplied by a numerical factor which scales roughly like $\mu/[(b - a)\bar{\sigma}]$, where μ is the shear modulus. If we take values μ = 30,000 MPa, $b - a$ = 0.004, and σ = 50 MPa, then h_{nucl} is of order $10^5 L$. Using $h_{\mathrm{nucl}} \sim 1$ m, we infer $L \sim 10$ μm, consistent with laboratory measurements. The fact that laboratory values of L are consistent with the sizes of smallest events on real faults can hardly be a coincidence.

[21] Hence L is likely to be in the laboratory range on the faults for the purpose of nucleation, otherwise small events could not occur. Since L is a material property, the same values of L should apply for nucleation of large events as well. This assumes that small as well as large events nucleate as frictional instabilities and that large events nucleate in the same places as small events and hence are governed by the same frictional properties. There is no physical reason to assume that, during nucleation, frictional properties for small and large events are different. One often used argument points out that characteristic slip distance L likely depends on roughness and concludes that large-scale roughness, and hence large L, must be appropriate for large earthquakes. However, the very relevance of the large-scale roughness to frictional processes in earthquakes is not established, as some studies of the fault structure [e.g., *Chester and Chester*, 1998] suggest that slip localizes during earthquakes (much like it does in the laboratory) and most of the slip is accommodated within the "prominent fracture surface".

[22] Much larger values of a frictional length scale, of order meter, are usually inferred from seismic inversions [e.g., *Ide and Takeo*, 1997; *Olsen et al.*, 1997]. These values are 4–6 orders of magnitude larger than the values of L observed in the laboratory. What can cause such a huge discrepancy? Most likely, a combination of several factors:

[23] 1. Frictional weakening distances are inferred using information about a seismic event as a whole. At large slip velocities and slips, ruptures are bound to be affected by processes other than rate and state frictional effects, such as pore pressure evolution, partial melting, and off-fault damage. These processes are likely to result in larger effective critical slip-weakening displacements during dynamic rupture (however, these larger critical displacements are likely irrelevant during nucleation). While many of these processes are caused by friction through frictional heating, they (and their effects on the rupture propagation and arrest) can hardly be adequately represented by simply increasing, in an arbitrary fashion, the characteristic slip distance of a friction law during the dynamic phase. Rather, physically based constitutive descriptions of these processes should be added to earthquake models. Such analysis is not a goal of this paper, but should be included in future studies.

[24] 2. The process of inferring frictional distances may have bias toward larger values due to filtering out high-frequency seismic data and numerical resolution issues during forward modeling, as discussed by *Uenishi and Rice* [2003].

[25] 3. Frictional distances are usually inferred From seismic inversions using linear slip-weakening laws, while the laboratory values are often reported for rate and state formulations. At the tip of the propagating rupture, rate and state friction maps into a nonlinear slip-dependent law with significant initial strengthening followed by almost linear weakening. The critical slip-weakening displacement L_{SW} of that effective slip-dependent law is about 15 times larger than the characteristic slip distance of the underlying rate and state formulation, $L_{SW}/L \approx 15$, as shown by *Cocco and Bizzarri* [2002] and verified by our simulations. This factor can account for a part of the discrepancy. We note here that the rate and state formulation has advantages in comparison with the slip-dependent one: the rate and state ideas are supported by ample laboratory evidence, account for rate dependence of friction, and model gradual regain of strength in stationary or nearly stationary contact.

[26] Since the emphasis of this paper is on nucleation and early dynamic propagation, one of our goals is to study the response of the model to progressively smaller values of L.

3. Small Events at Transition From Locked to Creeping Regions

3.1. Appearance of Small Events for Smaller Values of Characteristic Slip Distance

[27] As L decreases, small events appear near the brittle-ductile transition at the bottom of the seismogenic (velocity-weakening) zone, where there is a change to velocity-strengthening friction at deeper (hence hotter) locations on the fault. By a "small event" we mean an event that has not ruptured the whole seismogenic depth, whereas the term "large event" is used to refer to a model-spanning event (which in a 3-D model could further grow by propagating

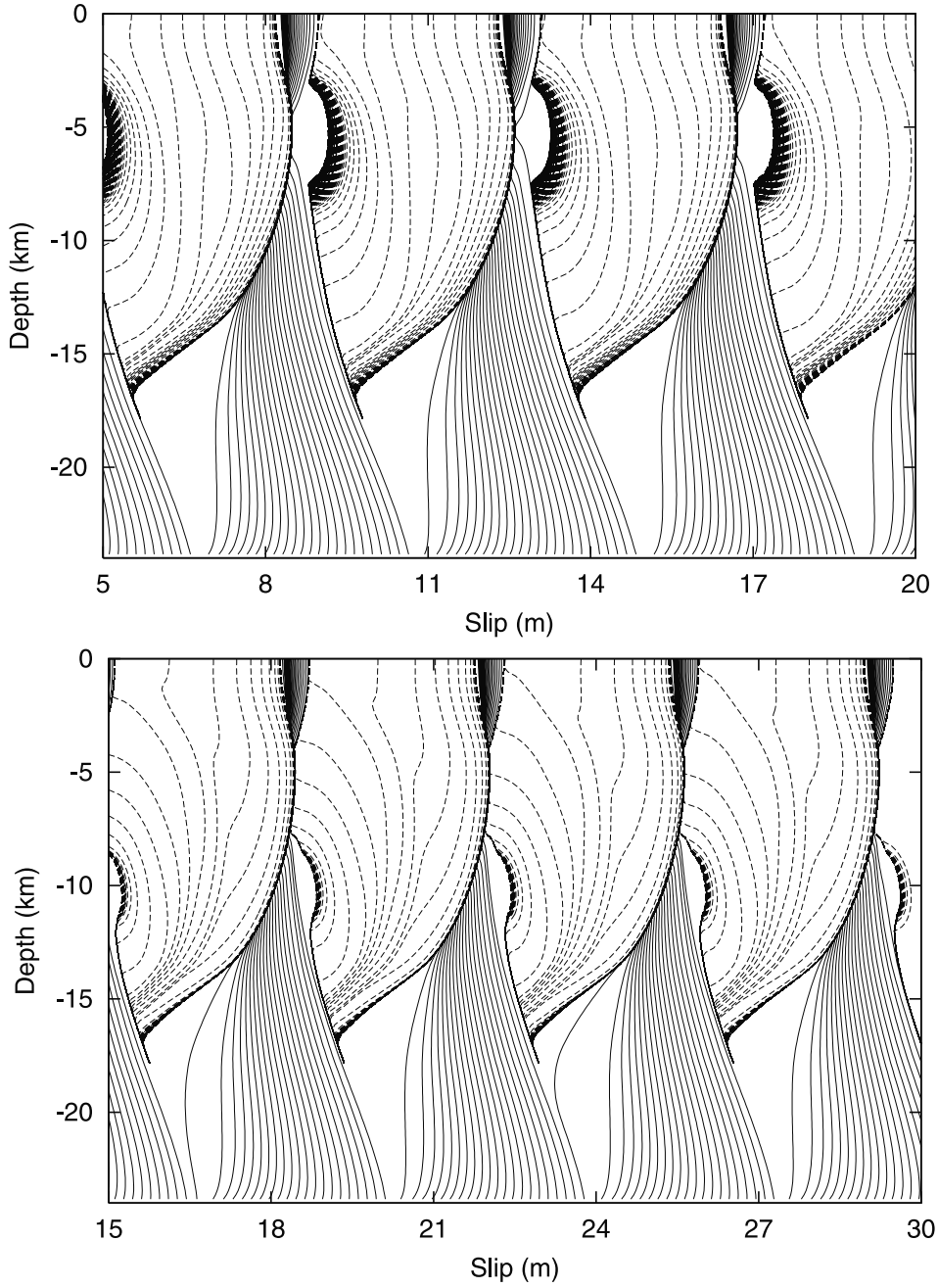

Figure 3. Slip accumulation for (top) L = 16 mm and (bottom) L = 8 mm. Each line represents the profile of slip at a certain time. The solid lines show slip accumulation every 5 years. The dashed lines are intended to capture model earthquakes and are plotted every second when maximum velocity on the fault is above 1 mm/s. For these large values of L, we get sequences of periodic events spanning the whole model.

along the strike). That is, we use words "small" and "large" to denote a qualitative difference between events.

[28] Simulations with L = 16 mm and L = 8 mm produce a periodic sequence of large events (Figure 3), while a simulation with L = 2 mm results in the sequence of a large and a small event (Figure 4, top). A simulation with L = 1 mm also results in the sequence of a large and a small event, similar to Figure 4 (top). Notice that with the decrease in L, the nucleation site of the events moves closer and closer toward the ductile-brittle transition at the bottom of the seismogenic zone.

[29] As mentioned in section 2.3, the size h_{nucl} of the nucleation region scales with L, being approximately proportional to L, but multiplied by a numerical factor which scales roughly like $\mu/[(b-a)\bar{\sigma}]$, where μ is the shear modulus, so that here h_{nucl} is of order $10^5 L$. Thus, according to this estimate, h_{nucl} is of order 1 m when L = 10 μm, while for the cases illustrated so far, with L = 16, 8, and 2 mm, the estimate results in h_{nucl} of order 1.6, 0.8, and 0.2 km, respectively, all rather large values. The sizes of the nucleation zones, obtained from simulations, are $\sim$5.5, 3.2, and 0.8 km, respectively, or $\sim$4 times larger

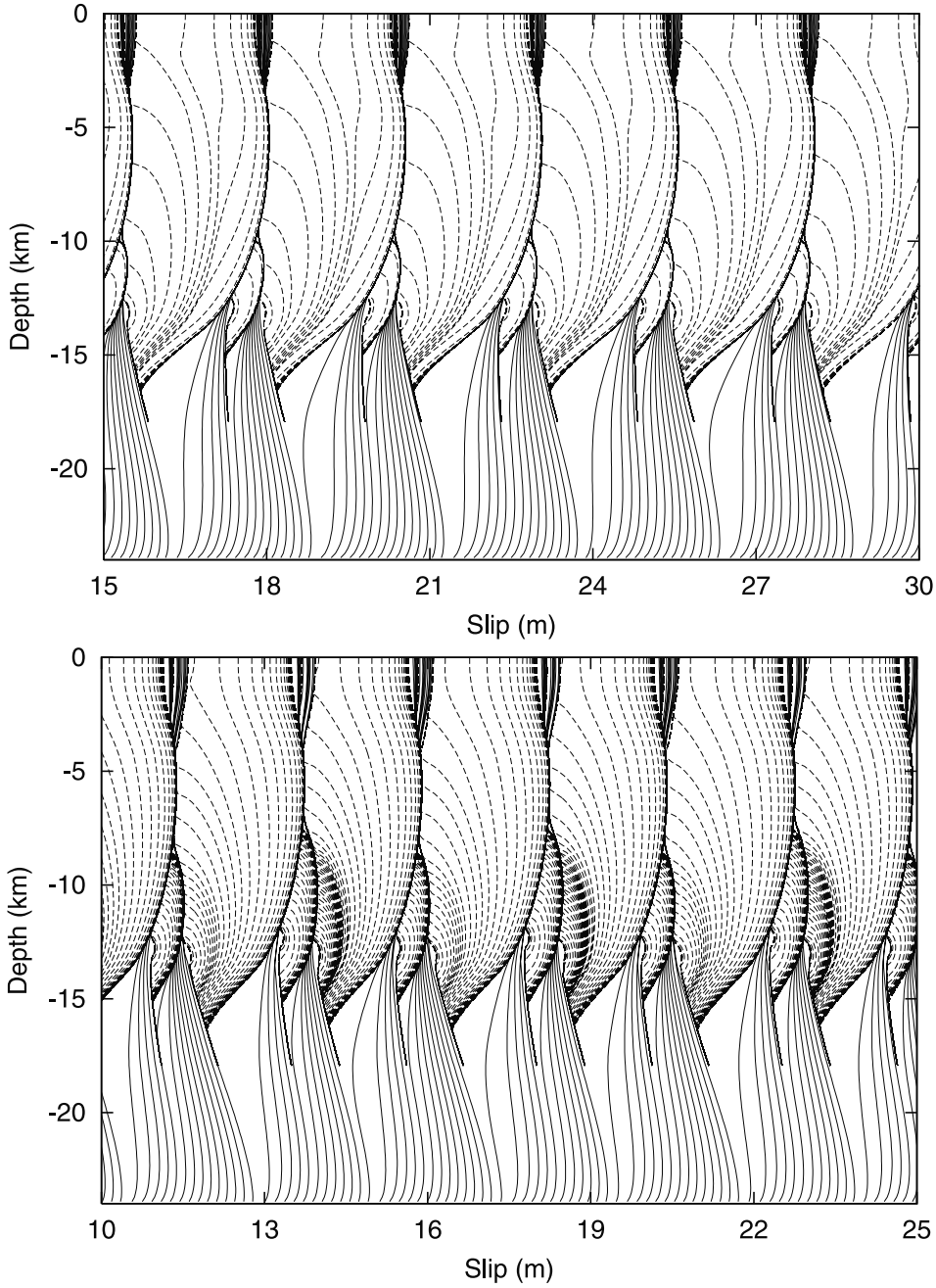

Figure 4. Slip accumulation for $L = 2$ mm with (top) all dynamic effects included and (bottom) dynamic stress transfers ignored (quasi-dynamic approximation). Lines have the same meaning as in Figure 3. Notice that a small event appears toward the bottom of the seismogenic zone.

than the estimate above. We note that the effective normal stress $\bar{\sigma}$ is taken here to vary with depth in a way that incorporates high fluid over pressurization at depth, and $\bar{\sigma} = 50$ MPa over most of the seismogenic (velocity-weakening) zone. For higher normal stress at depth, the nucleation size there would be smaller and slips per event would be larger.

[30] We have also simulated a still smaller value of L, $L = 0.14$ mm, which is within the range of some of the largest laboratory values, ~0.2 mm, ever reported [*Marone*, 1998]. We have reliable results for this case only within the quasi-dynamic approximation, as by *Rice* [1993]. The quasi-dynamic approach retains radiation damping, the dynamic feature that makes the solution exist during instability, but the stress transfers are modeled in a simplified way, as if the stress changes due to slip were the static changes and were propagated instantaneously.

[31] Note that the quasi-dynamic approximation works rather well in this model for larger values of L, preserving many important features of earthquake sequences we wish to observe. One comparison was given by *Lapusta et al.* [2000], for the sequence of large events with $L = 8$ mm. For another illustration, this time involving small events, consider Figure 4 (bottom), which shows the case of Figure 4

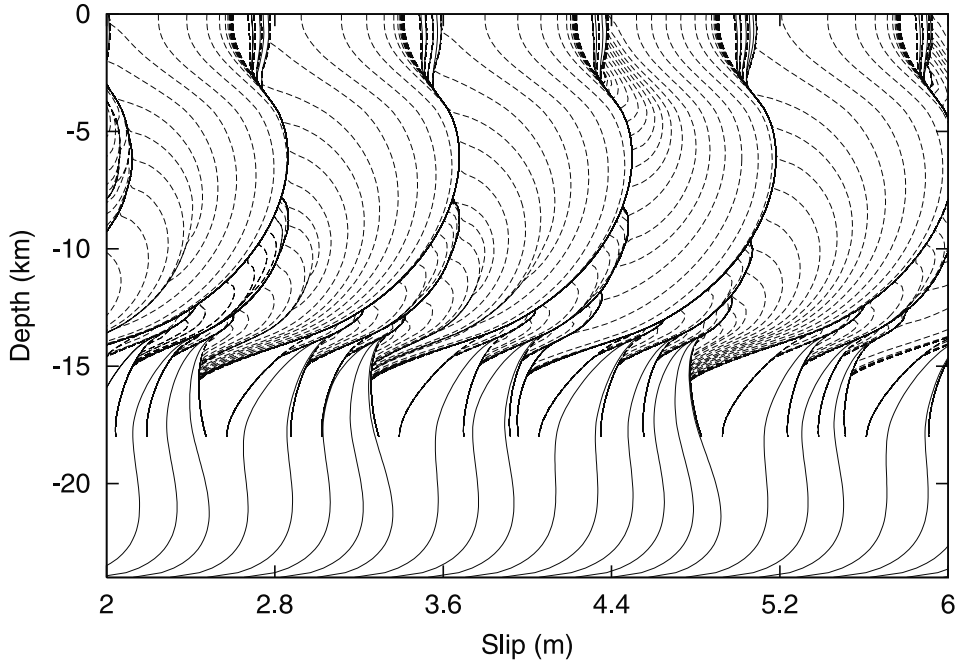

Figure 5. Slip accumulation for $L = 0.14$ mm, with dynamic stress transfers ignored (quasi-dynamic approximation). The distribution of the direct effect coefficient a is slightly modified, with a taken larger in the region of about 1.5 km next to the free surface (to allow for larger time steps during aseismic periods). The sequence of events is more complex, consisting of a large event, a small event, an intermediate event, and another small event.

(top), where $L = 2$ mm, but redone with the quasi-dynamic approach. We see that the main features are preserved, such as the nucleation phase, and the sequence of large and small events. There are also differences, in that the events are more sluggish, with noticeably smaller rupture velocity and slip velocity, and the slip per larger event is smaller. Also the event recurrence is periodic but now with two large and small events per full period that are similar but not fully

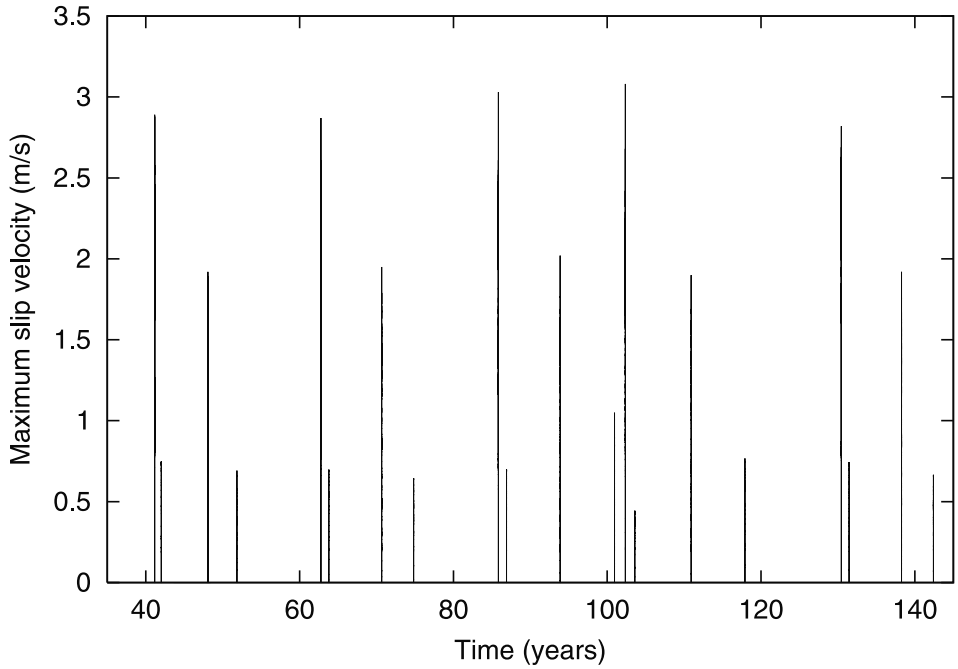

Figure 6. Maximum slip velocity on the fault for $L = 0.14$ mm (with quasi-dynamic approximation). Since each dynamic event lasts seconds, individual events are represented by straight lines on the timescale of the plot. The sequence of events is more complex, consisting of a large event, a small event, an intermediate event, and another small event. Note that slip velocities are slower in quasi-dynamic modeling than in modeling with full inclusion of inertial dynamics.

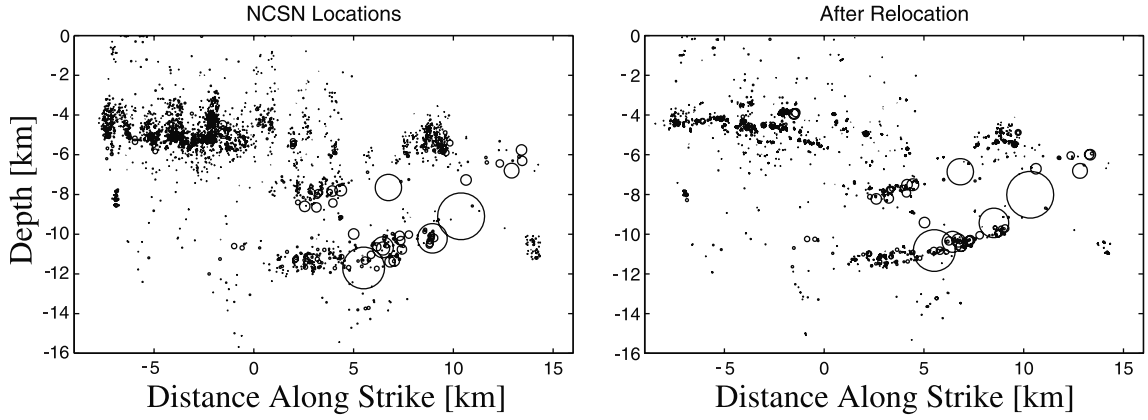

Figure 7. From *Ellsworth et al.* [2000], courtesy of W. L. Ellsworth. A longitudinal cross section of San Andreas fault seismicity in the Parkfield region from 1984 to 1999, with catalog locations on the left and more precise relocations on the right. The part of the fault starting at about 0 km along strike and extending to the right has two prominent semihorizontal streaks of small events. The 1934/1966 main shock hypocenter is located at the depth of 9.3 km at 5 km distance along the profile. *Ellsworth et al.* [2000] conclude that the zone between the streaks is locked, and the streaks outline the transition from locked to creeping behavior.

identical (one large event of the period very nearly arrests in the beginning of its propagation).

[32] The case of $L = 0.14$ mm, done only quasi-dynamically, shows further complexification of the model response. The sequence changes to that of a large event, a small event, an ''intermediate'' event, and another small event (Figure 5). Figure 6 shows the change in the model behavior in a more straightforward way, showing the maximum velocity on the fault as a function of simulated time in years. On such a plot, each event collapses onto a single line. That maximum velocity, during unstable events, is typically controlled by elements at the crack tip, and is slower for quasi-dynamic cases like this one than for full dynamics.

[33] The sequence for $L = 0.14$ mm does not look consistently periodic, mostly because of an occasional large event that starts at the top of the seismogenic zone rather than at the bottom, like the large event at around 4.4 m of slip in Figure 5 (or at about 102 years of simulated time in Figure 6). This is likely to be the consequence of compromises of parameters that we had to make to study such a small value of L (despite the compromises, and the fact that this is only a quasi-dynamic analysis, the problem was still very large, i.e., the number of space elements, including those needed for the mirror image, was 65,536 and each element represented about 1.1 m of depth). In particular, we decreased the replication distance in the depth direction from 192 to 72 km (the replication distance enters our modeling because we use FFTs). Such a decrease influenced in the same way the quasi-dynamic run with $L = 2$ mm, causing occasional large events to nucleate at the top. Note that the spot at the top transition from velocity strengthening to velocity weakening is a likely candidate for nucleation.

[34] Comparing Figures 3, 4, and 5, we see that smaller values of L introduce more elaborate sequences, with small events. Note that the qualitatively changing character of event sequences with decreasing characteristic slip distance L implies that simulating realistic values of L is important as the results may qualitatively depend on the size of L.

[35] Slip per large event in the case of $L = 0.14$ mm is about 0.8 m, which is much less than slips accumulated in large earthquakes in the Earth's crust. This is due to several factors in present modeling. The model presented is two-dimensional and large earthquakes in this model arrest shortly after reaching the free surface. In a 3-D model, the ruptures could continue to grow even after reaching the free surface, propagating along the strike and probably accumulating much more slip. This means that our large events cannot be compared to the largest earthquakes on reals faults, but rather to moderately large earthquakes. The value of the effective normal stress at depth is taken somewhat low, 50 MPa, and that too significantly reduces the amount of accumulated slip per event. The value of the effective normal stress chosen is easier to simulate and represents high fluid over pressurization at depth. Finally, and maybe most importantly, this modeling does not include processes that occur at large slip velocities and/or slips, such as additional weakening due to pore pressure evolution, flash heating, and partial melting. These processes should cause significant additional slip for any value of the frictional length scale and could introduce additional weakening length scales which are much larger than those of the rate and state effects.

3.2. Clustering of Small Earthquakes on Real Faults

[36] It is likely that on real fault segments that have locked patches, small events might cluster at the transitions from locked to creeping regions. An obvious such transition would be at the bottom of the seismogenic zone. It is not easy to find evidence to either support or refute this proposition. Event locations of sufficient accuracy are hard to obtain; also, establishing which fault segments are locked and which are creeping is by no means a solved problem, and often there is no consensus. However, some cases do provide supporting evidence, of which we will mention two, suggested to us by W. L. Ellsworth (private communication, 2001).

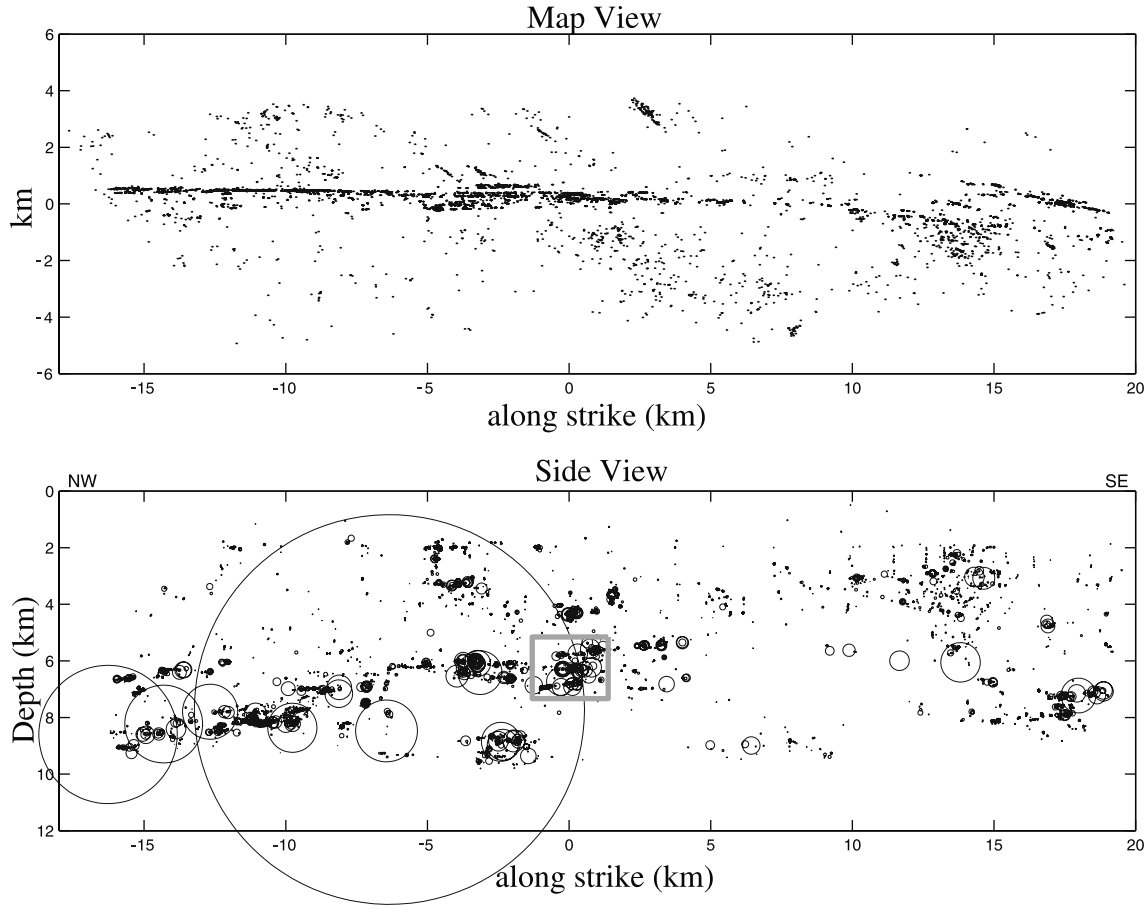

Figure 8. From *Schaff et al.* [2002], courtesy of D. P. Schaff. Earthquake locations for the Calaveras fault from 1984 until present, comprising 7857 events. (top) Map view of events along the Calaveras fault. (bottom) Fault plane side view displaying only on-fault earthquakes with estimated source sizes based on circular crack model using a 3 MPa stress drop. The largest event is the *M* 6.2 Morgan Hill 1984 main shock. The hole in microseismicity, outlined by small events, is located starting from about 4 km along strike and farther to the right. This was also the area of the largest slip during the Morgan Hill event.

[37] One such case comes from the studies of the Parkfield segment of the San Andreas fault in California, done by *Ellsworth et al.* [2000]. The largest events there are M 6 that repeated in the region from 1857 up to the latest in 1966. The hypocenters of the last two events (in 1934 and 1966) were located within a zone that is defined by two prominent lineations of microseismicity, one above the zone and one below (the zone is shown in Figure 7). Ellsworth et al. conclude that the zone is locked and these lineations are the loci of earthquake nucleation situated at the transition from locked to creeping behavior. They point out that this conclusion is supported by models of some small events from the region by *Fletcher and Spudich* [1998], in which slip initiates within the lineations and propagates into the zone containing the 1966 hypocenter.

[38] Another case is from the Calaveras fault in California, where there is a "hole" in small event seismicity shown in Figure 8 [from *Schaff et al.*, 2002]. *Schaff et al.* [2002] point out that this hole was the location of the area of greatest slip during the 1984 Morgan Hill Earthquake, as determined by *Beroza and Spudich* [1988], and hence this zone is most likely locked, with the small events around it outlining a transition from the locked zone to the creeping zones around. Similar conclusions were reached by *Oppenheimer et al.* [1990], who, however, had to contend with more poorly resolved locations of events. We can also notice clusters of events around 8 km depth to the left and right of that hole; these could possibly represent a transition to hot stable sliding at depths below the lineation defined approximately by those clusters.

3.3. Similarity of Nucleation Process for Small and Large Events

[39] The appearance of small events for smaller values of the characteristic slip distance L allows us to compare the nucleation process for large and small events. By "nucleation process" here we specifically mean the quasi-static slip (i.e., slip with negligible inertial effects) in a small slowly expanding zone before the breakout of the dynamic event, as it has been understood in theoretical studies of frictional instability. We observe this nucleation in our simulations, as discussed below. The transition to inertial slip (with high, seismic slip velocities) is accompanied by the rapid expansion of the slipping zone, with rupture

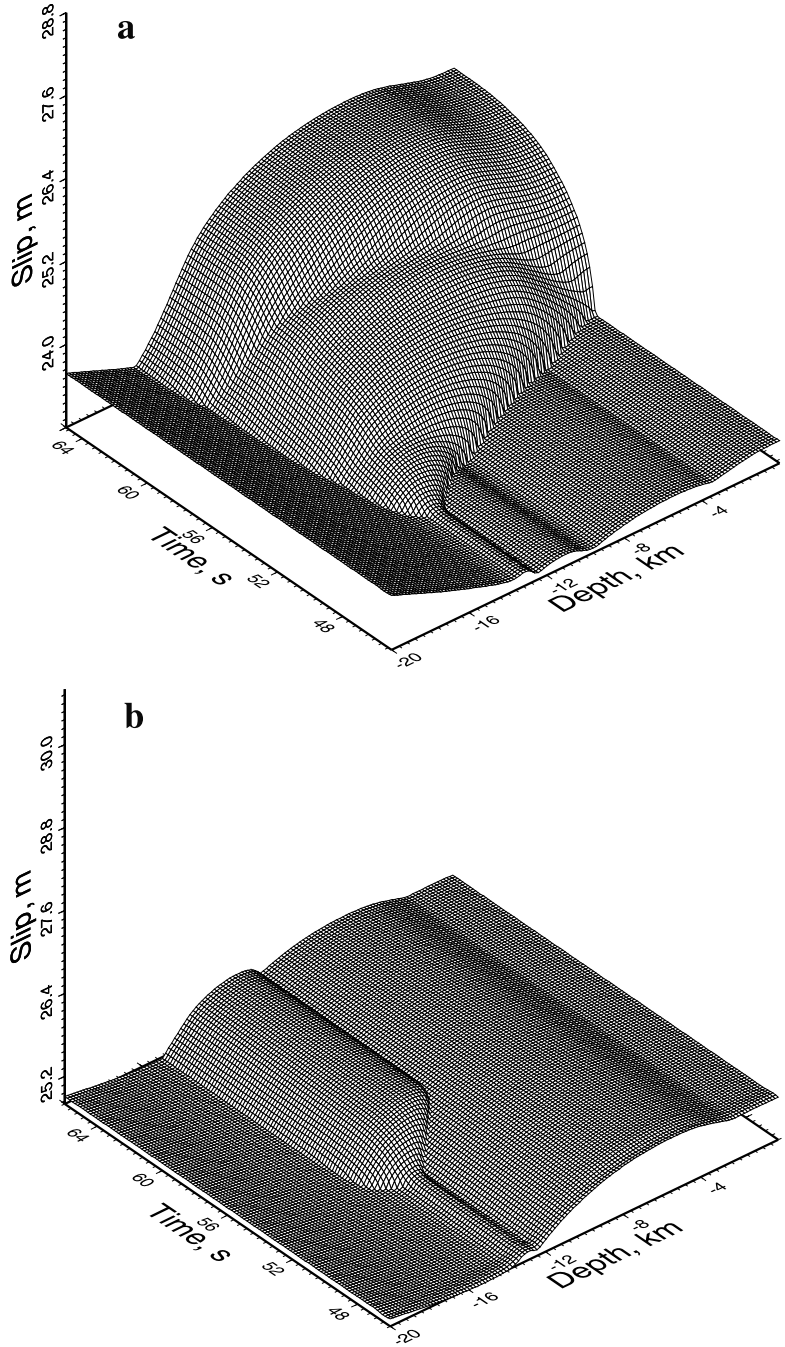

Figure 9. Slip in individual events from the sequence in Figure 4 (top), $L = 2$ mm, for (a) a larger event and (b) the following smaller event. The time axis spans 20 s, with zero time chosen arbitrarily for plotting convenience. The slip axis spans 6 m in both cases. Notice the clear nucleation zone that extends much further back in time. The beginning of the smaller event in Figure 9b looks just like the beginning of the larger event in Figure 9a; it stops by not being able to advance into the higher slip/lower stress region in the middle of the fault. This supports the idea that large events are small events that run away due to favorable stress/strength conditions on the fault. From *Lapusta et al.* [2000].

velocities that are a significant fraction of the shear wave speed. In our definition, this expansion signals that the nucleation phase has ended and dynamic rupture propagation has begun. This contrasts with use of the term "nucleation phase" to denote the early seismically detectable signals of an unstable rupture, like by *Ellsworth and Beroza* [1995], and we would urge that such be always denoted as the "seismic nucleation phase."

[40] We can compare the nucleation and beginning of the larger and the smaller events for the case $L = 2$ mm (Figure 4, top) by considering plots of slip (Figure 9) for individual large and small events of the sequence. Note that more than

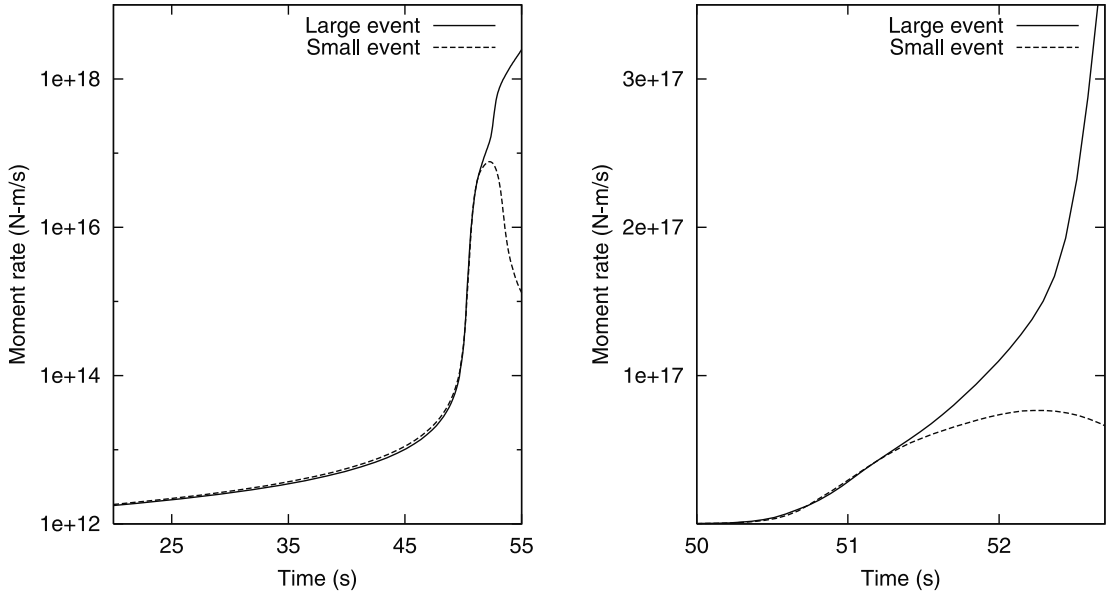

Figure 10. Comparison of moment rate, as a function of time, for the large and small events shown in Figure 9. Zero in time is chosen arbitrarily for plotting convenience. The signal from the beginning of the two events is very similar.

20 meters of slip was accumulated in this simulation before the events shown. We can distinguish a nucleation zone that precedes the model earthquakes. The nucleation and beginning of both events look very similar. The similarity is also evident on the corresponding slip velocity plots [*Lapusta et al.*, 2000].

[41] To quantify the similarity, we plot in Figure 10 the moment rate released in both large and small events in the beginning of the events. (The moment calculations are explained in section 4.1.) Figure 10 (left) plots the moment rate on a logarithmic scale, to allow for comparison of the moment rate released before the dynamic phase of the events. We see that the moment rate at the last stages of the nucleation (from 20 to ~50 s on the plot) is virtually identical. In Figure 10 (right), a linear scale for the moment rate axis is used, to concentrate attention on the beginning of the dynamic phase. The moment released at the early stages of the dynamic propagation (from ~50 to ~51.2 s) is again virtually identical for the two events.

[42] Hence the nucleation (as defined in the beginning of section 3.3) and initial propagation of the large and small events in our simulations is very similar, as manifested by plots of slip (Figure 9), slip velocity [*Lapusta et al.*, 2000], and moment rate (Figure 10). One would not be able to determine the final size of such a model earthquake by observing the signal from its nucleation and early seismic propagation. The final size of a simulated event is not dictated by the nucleation process, but rather by the conditions further along the fault.

4. Irregular Moment Release of Large Events

4.1. Moment Rate and Acceleration Calculations

[43] To quantify the signal from the nucleation and initial stages of dynamic rupture propagation, we compute moment acceleration. Note that the source signal (i.e., the signal with path and receiver effects ignored) for velocity seismograms in the far field is proportional to the moment acceleration [e.g., *Aki and Richards*, 1980]. Moment cannot be usefully discussed in the 2-D model where slip extends infinitely, and simultaneously, along strike at any given depth. We therefore use our 2-D modeling to provide input to a 3-D source in such a way that maps the 2-D slip distribution into a 3-D one. The procedure used would be exact (except for a numerical prefactor) if applied to known solutions for cracks of constant stress drop which grow at constant rupture velocity V_r; in both 2-D and 3-D solutions of this type, slip is proportional to $(V_r^2 t^2 - r^2)^{1/2}$, where r is the distance from the rupture origin. We note that in our case neither stress drop nor rupture velocity are constant.

[44] If we let $r = (x^2 + z^2)^{1/2}$, with x and z measured from some suitable origin, then, for a 3-D source with the radial symmetry property $V(x, z, t) = V(r, t)$, we have for the moment rate

$$\dot{M}_0(t) = \mu \int\int V(x,z,t)dxdz = 2\pi\mu \int_0^{r_{\max}} V(r,t)rdr. \qquad (3)$$

We select the center of the nucleation zone as the effective origin z_o and reinterpret the above integral in terms of the computed slip velocity $V(z, t)$ from our 2-D modeling as

$$\dot{M}_0(t) = \pi\mu \int_{z_{\text{bottom}}}^{z_{\text{top}}} V(z,t)|z - z_o|dz. \qquad (4)$$

We filter out numerical noise by averaging $\dot{M}_0(t)$ in small time intervals (which are ~0.07 s for the cases considered here). Moment acceleration $\ddot{M}_0(t)$ is then computed as

$$\ddot{M}_0(t) = d\dot{M}_0(t)/dt. \qquad (5)$$

We have used this procedure in section 3.3 to compute moment rate for the nucleation and beginning of a large and

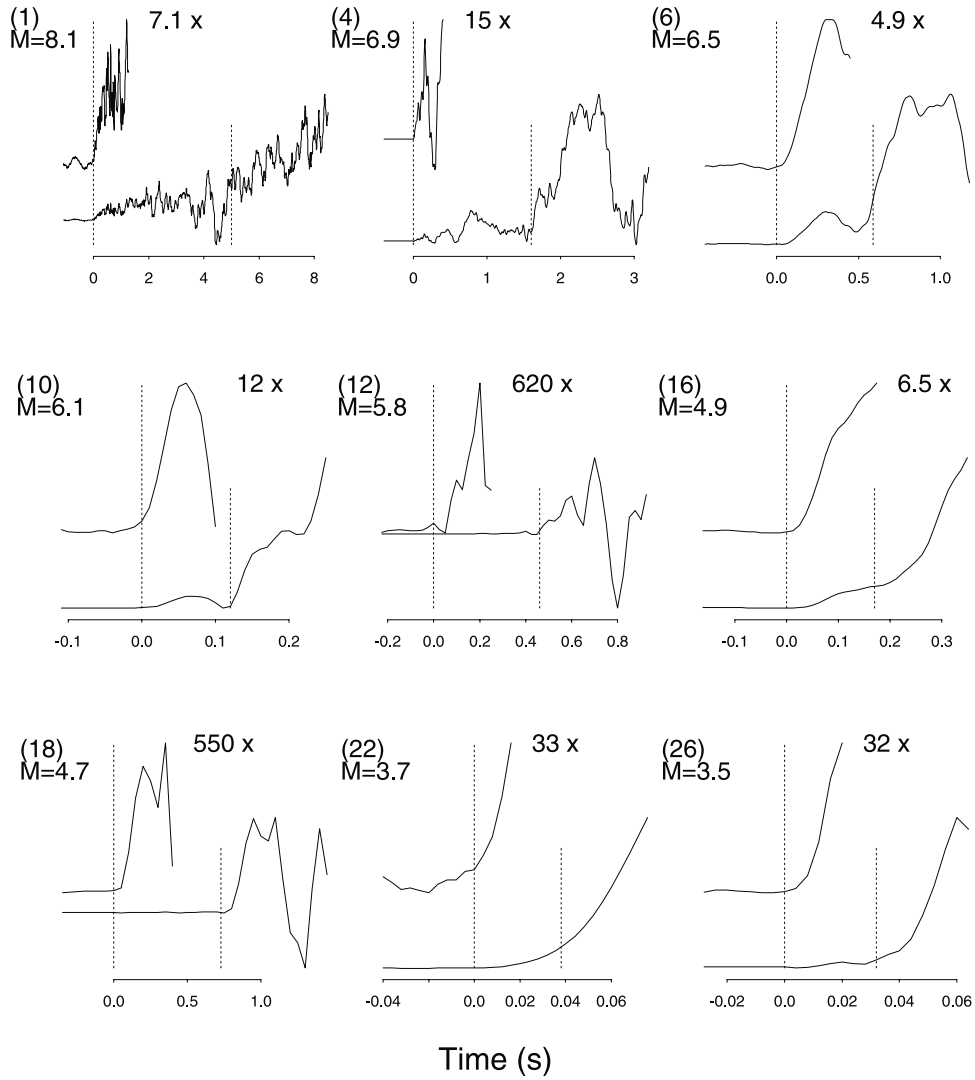

Figure 11. Broadband velocity seismograms are shown at two amplitude scales to display the character of the first arrival and the subsequent strong arrivals. Time increases from left to right and is at different scale for each seismogram. Note slowdowns and speedups in the initial phases, similar to model earthquakes in Figure 13. Reprinted with permission from *Ellsworth and Beroza* [1995] (copyright 1995 American Association for the Advancement of Science), courtesy of G. C. Beroza.

a small events from the sequence with L = 2 mm (Figure 10). Specifically, we computed

$$\dot{M}_0(t) = \pi\mu \int_{-24\text{ km}}^{0} V(z,t)|z - z_o|dz, \tag{6}$$

where $z_o = -12.92$ km for the small event and $z_o = -13.03$ km for the large event (these values were estimated from the data used in Figure 9).

4.2. Moment Acceleration of Simulated Large Earthquakes

[45] Our study of initial moment acceleration is motivated by observations that many real earthquakes exhibit irregular moment acceleration in the beginning of their dynamic propagation, as shown by *Ellsworth and Beroza* [1995]. Figure 11 reproduces Figure 2 from *Ellsworth and Beroza* [1995] and shows velocity seismograms for several earthquakes. Figure 12 reproduces Figure 4 from the same paper, giving the moment acceleration itself.

[46] Moment acceleration for simulated large events from sequences with L = 8 mm and L = 2 mm (obtained in fully dynamic simulations) is shown in Figure 13. For each large event, we compute "full" moment acceleration, given by

$$\dot{M}_0(t) = \pi\mu \int_{-24\text{ km}}^{0} V(z,t)|z - z_o|dz,\ \ddot{M}_0(t) = d\dot{M}_0(t)/dt, \tag{7}$$

and "partial" moment acceleration, given by

$$\dot{M}_0(t) = \pi\mu \int_{z_o}^{0} V(z,t)|z - z_o|dz,\ \ddot{M}_0(t) = d\dot{M}_0(t)/dt, \tag{8}$$

where, as before, z_o is the center of the nucleation zone, estimated to be -10.14 km for the large event with L = 8 mm

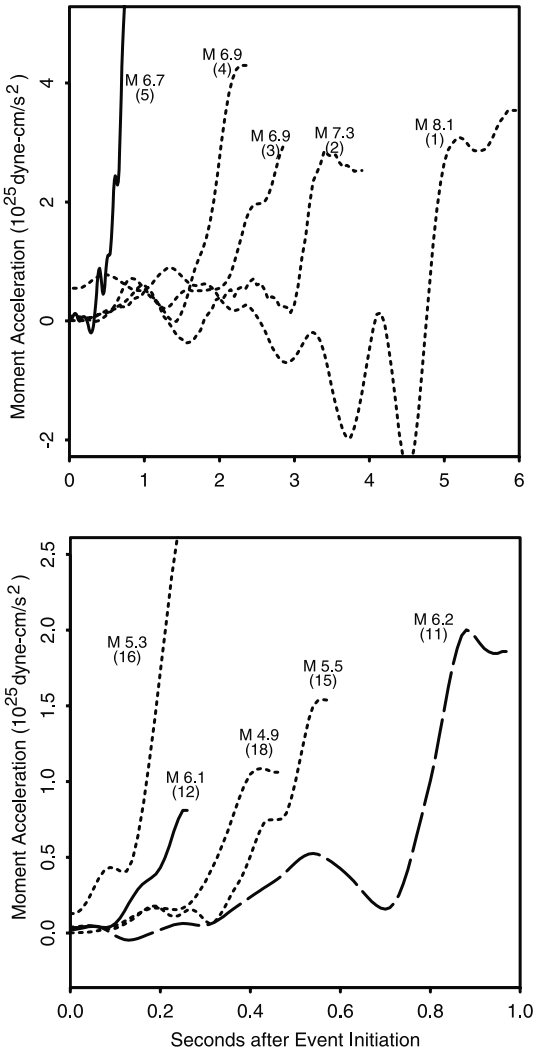

Figure 12. Moment acceleration functions for the initiation of earthquakes. The initial phases of the earthquakes exhibit irregularities, similarly to model earthquake in Figure 13, especially for events with the moment magnitude 5 to 6 shown in the bottom of this figure. Note that 10^{25} dyn cm/s^2 = 10^{18} N m/s^2. Reprinted with permission from *Ellsworth and Beroza* [1995] (copyright 1995 American Association for the Advancement of Science), courtesy of G. C. Beroza.

and −13.03 km for the large event with L = 2 mm. Partial moment acceleration accounts only for the part of the rupture that runs from the nucleation zone to the free surface (the "first" rupture front). The difference between full and partial moment acceleration values shows the contribution from the other part of the rupture, which runs from the nucleation zone to the velocity-strengthening region at depth (the "second" rupture front), where it arrests.

[47] We see that, for both events, the moment acceleration exhibits a "bump," that is, a speedup (segments AB for the event with L = 2 mm and NP for the event with L = 8 mm), then a slowdown (segments BC and PQ), and then another speedup (segments CD and QR), similarly to observations (Figures 11 and 12). However, as discussed in the following, the "bumps" are caused by different reasons for the two events. The important differences between the two events are that the event with L = 8 mm starts farther from the velocity-strengthening region (and hence its partial arrest in the velocity-strengthening region has significant effect), while the event with L = 2 mm comes from the sequence that has small events (and hence it encounters stress concentration left by arrest of the previous small event).

[48] We note that model earthquakes in this 2-D model should be compared to moderately large real events, because, due to the character of our 2-D depth-variable model, they arrest shortly after running through the crustal depth and hitting the free surface, whereas in a 3-D context, an event could keep growing by propagating along the strike.

4.3. Influence of Stress Concentration Due to Prior Small Events and Creeping Regions

[49] Let us consider first the large event from the simulation with L = 2 mm (Figure 13b) which has small events. We see that full and partial moment acceleration (given by solid and dashed lines, respectively) is virtually the same, reflecting the fact that the event starts very near the velocity-strengthening region at the bottom of the fault. Hence the "bump" ABC results as the rupture propagates from the nucleation zone up to the free surface (the "first" rupture front). From the dashed line of Figure 13a, we see that the "first" rupture front of the event with L = 8 mm does not produce such a bump.

[50] Hence the bump ABC is conjectured to be caused by rupture propagation over the heterogeneous shear stress field left by the previous small event. To confirm this, as well as to understand other features of the moment acceleration, we plot in Figure 14 shear stress before the large event for the case L = 2 mm. We see that there are three places of stress concentration. The first place is at about −12.5 km, and corresponds to the tip of the creeping zone at the bottom of the fault. That part of the plot is enlarged in the inset (which also serves to show the high degree of numerical resolution of the features shown). We see that there are two peaks in stress there. The one at about −12.6 km corresponds to an end of the nucleation zone (the spatial extent of the nucleation zone is shown by a short thick solid line). The other one, at about −12.5 km, corresponds to the end of the zone that was creeping before the event (even though this part of the fault has velocity-weakening properties, a sufficiently small slipping zone can only creep). The second place of stress concentration is from about −10.5 to −8 km. This stress concentration is caused by arrest of the previous small event (the spatial extent of the small event is shown by a longer thick solid line). Note that the dynamic propagation of that small event ended at about −10 km, and the slipped zone got extended to about −9.5 km through postseismic creep. The points A, B, C, etc., on the plot show spatial positions of the "first" rupture front at times corresponding to the markings in Figure 13b. That is, point A in Figure 13b corresponds to 52.34 s and to the beginning of the speedup AB; point A in Figure 14 indicates at that time (52.34 s) the rupture front was at about −10.5 km or at the beginning of stress concentration left by arrest of the small event. Similarly, point B in Figure 13b denotes the time of the highest moment acceleration in the bump; point

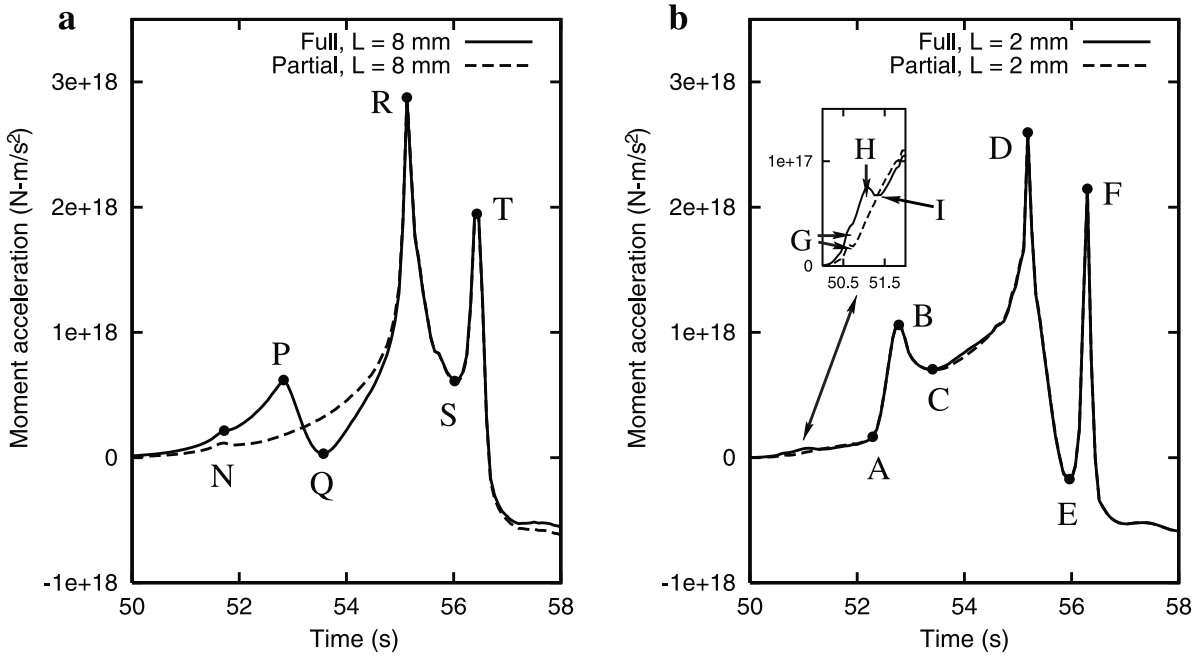

Figure 13. Moment acceleration in large events from sequences with (a) $L = 8$ mm and (b) $L = 2$ mm. Full moment acceleration accounts for the whole rupture propagation, while partial moment acceleration is computed only for the part of the rupture that runs from the center of the nucleation zone to the free surface. Note "bumps" in moment acceleration during early stages of rupture propagation, NPQ in Figure 13a and ABC in Figure 13b, similar to observations (Figures 11 and 12). The moment acceleration is 0.6×10^{15} N m/s^2 at 50 s and 0.7×10^{17} N m/s^2 at 51 s.

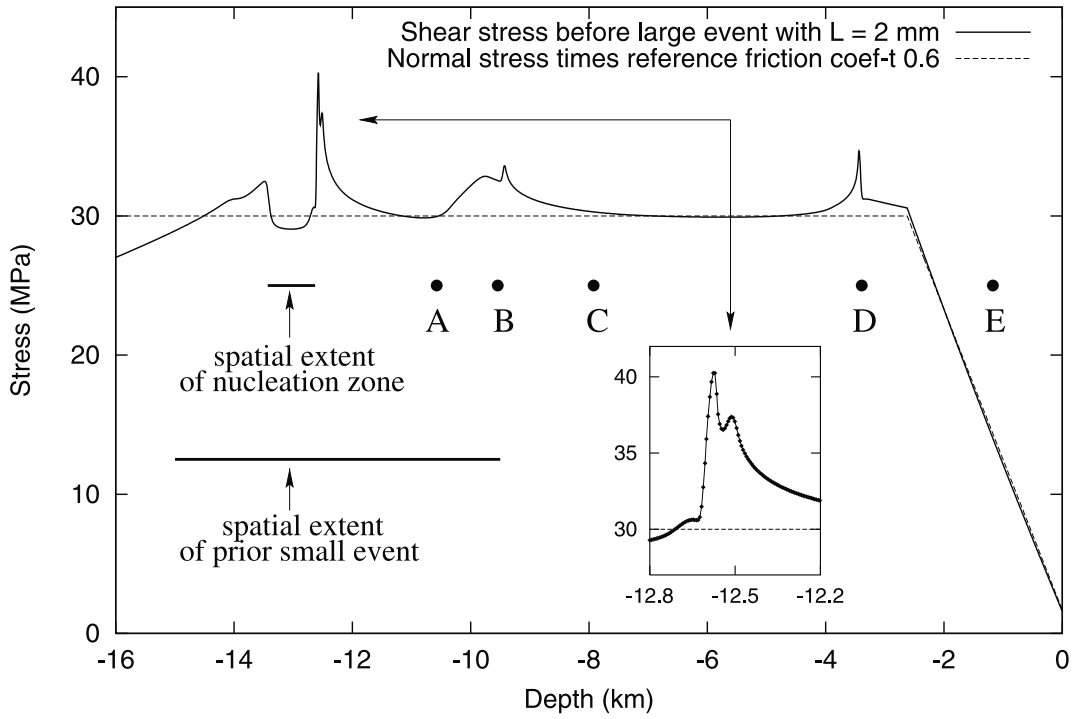

Figure 14. Shear stress distribution on the fault before the large event from the sequence with $L = 2$ mm. Points A, B, C, D, and E show positions of the rupture front at times corresponding to markings in Figure 13b as explained in the text. Note stress concentration caused by arrest of the prior small event as well as by ends of creeping zones (the nucleation zone and the zone creeping next to the free surface). The features in stress distribution have direct correspondence to features of moment acceleration during the event (Figure 13b).

B in Figure 14 shows that the rupture front at that time was passing through the region of the highest stress of that stress concentration. The end of the bump in moment acceleration (point C) is related to the end of the region with concentrated stress.

[51] Finally, the third place of stress concentration is at −3.5 km and it corresponds to the end of the creeping zone next to the free surface. This place of stress concentration corresponds to a peak in moment acceleration (point D). Afterward, moment acceleration decreases due to the rupture propagation over the velocity-strengthening region next to the free surface; the local minimum E in moment acceleration corresponds to the rupture front being at about −1.3 km. Moment acceleration increases as the rupture approaches the free surface (F in Figure 13b), at which point our moment computation approximating a 3-D source is no longer sensible. As mentioned before, shortly afterward the event arrests, whereas in a 3-D context it could keep going by propagating along strike. In section 4.5, we remark on the applicability and limitations of approximating a 3-D source with 2-D data, using this place of stress concentration as an example.

[52] There is a slight difference between the full and partial values in the very early moment acceleration, as shown in the inset in Figure 13b. We will discuss the small "bump" in the solid line (denoted by GHI, at about 51 s) in section 4.4. There is another tiny bump in that inset, in both full and partial values, denoted by G. This bump corresponds to rupture propagation over the region of stress concentration at the end of the zone that was creeping before the event (shown in the inset in Figure 14, at about −12.5 km). The effect of this stress concentration on the moment acceleration is small, because the rupture nucleates just before propagating over that region and the overall moment acceleration is small.

[53] Moment acceleration in a large event from the case L = 8 mm (shown in Figure 13a) can be analyzed in a similar way. In particular, features that coincide for both full and partial moment computation are caused by rupture propagation from the nucleation zone to the free surface. We can establish that peak R in the moment acceleration is analogous to D and corresponds to rupture propagation over the area of stress concentration at the end of the creeping zone adjoining the free surface. Similarly, the small bump around the point denoted by N, in the very beginning of rupture propagation, is present in both full and partial moment acceleration and, analogously to G, corresponds to rupture propagation over the region of stress concentration at the end of the zone that was creeping before the event (as we can see from Figure 3 (bottom), this end, located at about −7.8 km, is closer to the free surface than the end of the nucleation zone, which is at about −8.5 km).

[54] Hence we have established that the irregularity (bump) ABC in moment acceleration (of the event with L = 2 mm), a feature similar to observations, is caused by the rupture propagation over the region of stress concentration left by arrest of the previous small event. Note the abruptness of change in the rate of moment acceleration as the zone of stress concentration is encountered (point A). We have also linked other features (D, G, R, N) in moment acceleration of both events to stress concentration at ends of creeping regions.

4.4. Influence of Arrest in Velocity-Strengthening Regions

[55] As mentioned above, the difference between full moment acceleration (solid lines in Figure 13) and partial moment acceleration (dashed lines in Figure 13) gives the contribution of the part of rupture that runs from the nucleation zone to the velocity-strengthening region at the bottom of the fault (the "second" rupture font), where it arrests. This part of the rupture has very small effect on moment acceleration of the large event with L = 2 mm (Figure 13b), because in that sequence events nucleate very close to the velocity-strengthening region. In contrast, events from the sequence with L = 8 mm nucleate farther from the velocity-strengthening region, and hence the second rupture front has an opportunity to develop before its arrest in the velocity-strengthening region. Correspondingly, the contribution of this second rupture front in the case of L = 8 mm is much more pronounced, first adding substantially to the moment acceleration (segment NP of the solid line versus the corresponding part of the dashed line, Figure 13a), and then decreasing the moment acceleration as this second rupture front is arrested in the velocity-strengthening region at the bottom of the fault (segment PQ of the solid line). Hence the bump NPQ in moment acceleration is created. Note that similar effect, but on much smaller scale, happens in the event with L = 2 mm as well, creating a small bump GHI visible on the inset in Figure 13b.

[56] Even though the irregularity NPQ in moment acceleration of the event with L = 8 mm looks somewhat similar to the irregularity ABC of the event with L = 2 mm, it is clear that these two bumps are caused by totally different reasons: the first one (NPQ) is caused by the arrest of part of the rupture in the velocity-strengthening region at the (hot) bottom of the fault and the second one (ABC) is caused by stress concentration due to arrest of the prior small event. Since results for L = 2 mm are, apparently, representative of those for yet smaller L (all smaller L considered result in small events at the base of the seismogenic zone), we suggest that the L = 2 mm case may be more representative of natural events.

4.5. On Applicability and Limitations of Moment Acceleration Calculation

[57] Moment acceleration is computed here translating our 2-D fault model (fault 1) to a 3-D fault model with essentially radial symmetry on the fault plane (fault 2). This assumes that all features along the depth of fault 1 are present on fault 2 along a semicircle centered on the nucleation zone. This approximation certainly seems reasonable when rupture has not advanced much past the nucleation region, as in a 3-D context ruptures can certainly grow in a "circular" fashion, with radial symmetry, at least initially. Hence features such as a bump in moment acceleration due to the stress concentration left by arrest of a previous small event are most likely realistically represented. However, other features may be less adequately represented by this approach. In particular, features resulting from the fault structure, such as stress concentration at ends of creeping zones and arrest in velocity-strengthening regions, are not generically represented by semicircles on real faults. Hence they would not be encountered by the rupture over most of its front at once, as in our approximation, but rather their influence would be more gradual. For example, in the

case of stress concentration at about −3.5 km in Figure 14 (corresponding to the end of the zone creeping near the free surface, for $L = 2$ mm), our calculation essentially assumes that there is such stress concentration on a semicircle of radius $-3.5 - (-13) = 9.5$ km on the approximated 3-D source with the radial symmetry, which may be true, but is certainly not a generic feature of rheologic boundaries. Hence the effect of such stress concentrations may be overestimated in our moment calculation.

[58] Hence 3-D modeling is needed to fully establish the relative importance of features affecting moment acceleration. A 3-D simulation would also allow events to grow by propagating along the strike, resolving another limitation of 2-D modeling of large events. In addition, in such modeling (if it could be done for realistically small L), small events at the base of the seismogenic zone would leave heterogeneities in stress along strike, which the large events would pass through.

5. Conclusions

[59] We have considered nucleation and early dynamic propagation of model earthquakes in our simulations. Such studies are very important for understanding the physics of earthquakes, yet most methods are not applicable to these problems because they model appropriately either only the quasi-static slip during the nucleation phase or only the dynamic propagation phase. The methodology developed in *Lapusta et al.* [2000] and used here is ideally suited for the study of processes before, during, and after the nucleation of a model earthquake since it is able to simulate consistently the transition between the quasi-static and the dynamic slip, preventing the potential disruption of the simulated process of earthquake development. Still, these are extremely challenging computational problems, if to be addressed for the characteristic slip distance L close to the laboratory range.

[60] We have seen that smaller (and more realistic) values of L, if still large compared to typical laboratory values, produce small events in the simulated sequences. On the one hand, this is good news, as it lets us study small events and compare them, in particular their nucleation, to large events. On the other hand, it means that simulating realistically small values of L is important, as it qualitatively changes the model behavior. This is bad news, because simulating realistic values of L is very challenging numerically and hence is presently possible only in simple 2-D situations. Hence many important problems would have to be studied in a 2-D context. However, 3-D modeling is essential for confirming and clarifying features of 2-D modeling presented here.

[61] We note that the small events in our 2-D modeling do not increase nearly as fast with decrease of L as for one to expect that, with realistically small L, they could fill out a Gutenberg-Richter distribution for some range of small events in a 2-D model. (*Wesnousky* [1990, 1994] and *Stirling et al.* [1996] show that events plausibly associated with a major fault do have a G-R distribution over a range of smaller magnitudes.) Moreover, it is not clear whether further decrease of L will produce more small events. However, in the real 3-D Earth's crust, there are plenty of locations along strike for these small events to form, and 3-D modeling is necessary to understand how the change to 3-D affects the size distribution and event populations.

[62] The nucleation process of large and small events is very similar in our model. This means that, during the nucleation, we cannot decide whether the event will be large or small; large events start as small events and then grow due to favorable conditions further on the fault. This is not a trivial result, even for fixed frictional properties used in this study, because the strength of the fault in not fixed in the rate and state formulation and depends on the fault state (and hence slip) and slip velocity. Some researchers argue that events become larger because they get a stronger initial "push" from a larger nucleation zone [e.g., *Ohnaka*, 2000]. We show that the ultimate size of the event is not determined by the nucleation in this model. If this is what happens on fault zones in the Earth's crust, then, obviously, there is no hope that large earthquakes would ever be betrayed by the nucleation process, or that the nucleation process itself would be possible to detect. We remark below on possibilities to determine ultimate event size from the early seismic phases of moment release.

[63] In our simulations, large events have irregular moment acceleration in the beginning of dynamic propagation, exhibiting bumps (speedups and slowdowns), consistently with observations [*Ellsworth and Beroza*, 1995]. These irregularities result from rupture propagation over heterogeneous stress field caused by arrest of previous small events and creeping zones. The irregularities also result from partial arrest of ruptures in velocity-strengthening regions. It is important to understand limitations of interpreting 3-D data from 2-D modeling, as discussed in section 4.5. Still, it is rather surprising that even in such a simple model, with planar fault and with uniform frictional properties and normal stress in the seismogenic region, we can already observe these irregular features of moment acceleration. It seems reasonable to conclude that on real faults, with larger events nucleating in regions previously slipped in (a number of) smaller events and/or in regions close to transitions between locked and creeping behavior (which may not be sharply defined), the effects we have observed here in model earthquakes can play a significant role. Hence early moment acceleration may contain important messages about stress heterogeneity on the fault, as well as about possible heterogeneities of the fault structure. We note that other possible factors causing the irregularity of moment acceleration include, among others, off-fault phenomena such as branching and/or intermittent rupture propagation [*Poliakov et al.*, 2002], which we have not studied here and the signature of which still has to be explored.

[64] We must leave it as an open question, that our present work cannot resolve, if there are any differences in the early phases of seismic moment release, such as the length of these phases, that would make larger events look different from smaller ones. The understanding, developed here, of features affecting that moment release, in terms of patterns of stress heterogeneity left by prior small events and creep processes, would suggest that one would have to relate any such differences to factors of the prestress field. For example, if it could be argued that large events only occur after the stress landscape, cluttered with many failed smaller events, attains certain statistical properties different from what smaller events see, then the early phases of moment release of large events could have not only reluctant initial moment acceleration ("seismic nucleation phase") of longer duration (as

argued by *Ellsworth and Beroza* [1995]), but also features in that seismic nucleation phase that are qualitatively different from those of smaller events. It might also turn out, however, that even though larger events have more smaller events before them and hence potentially longer seismic nucleation phases, the appearance of that seismic nucleation phase is self-similar, so that smaller events are similar in appearance to (the beginning of) the seismic nucleation phase of larger events, and it would be impossible to distinguish whether the signal is a seismic nucleation of a large event or a smaller event about to end. Finally, it may turn out that reluctant initial phases of large and small events are similar both in character and duration, and observations of longer seismic nucleation phases for larger events as in *Ellsworth and Beroza* [1995] have alternative explanations, such as occurrence of subevents [*Kilb and Gomberg*, 1999]. As mentioned, 3-D modeling is needed to understand better how prestress and creeping regions affect moment acceleration, but computationally accessible 3-D modeling would probably not be able to distinguish, at least in the near future, between the scenarios outlined above, due to numerical limitations on the range of event sizes feasible to represent in such simulations.

[65] **Acknowledgments.** These studies were supported by the Southern California Earthquake Center (SCEC) and by USGS grant 99-HQ-GR-0025 to Harvard University. SCEC is supported by NSF Cooperative Agreement EAR-8920136 and USGS Cooperative Agreements 14-08-0001-A0899 and 1434-HQ-97AG01718. This is SCEC contribution 609. We are grateful to Bill Ellsworth, Rachel Abercrombie, Paul Segall, and Greg Beroza for insightful suggestions and discussions as well as to Mitsuhiro Matsu'ura and an anonymous reviewer for helpful comments. We also thank Bill Ellsworth, Greg Beroza, and David Schaff for giving the permission to use their figures and for providing digital copies of them.

References

Abercrombie, R., and J. Mori, Local observations of the onset of a large earthquake: 28 June 1992 Landers, California, *Bull. Seismol. Soc. Am.*, *84*, 725–734, 1994.

Aki, K., and P. G. Richards, *Quantitative Seismology: Theory and Methods*, W. H. Freeman, New York, 1980.

Ben-Zion, Y., and J. R. Rice, Dynamic simulations of slip on a smooth fault in an elastic solid, *J. Geophys. Res.*, *102*, 17,771–17,784, 1997.

Beroza, G. C., and P. Spudich, Linearized inversion for fault rupture behavior: Application to the 1984 Morgan Hill, California, earthquake, *J. Geophys. Res.*, *93*, 6275–6296, 1988.

Blanpied, M. L., D. A. Lockner, and J. D. Byerlee, Fault stability inferred from granite sliding experiments at hydrothermal conditions, *Geophys. Res. Lett.*, *18*(4), 609–612, 1991.

Blanpied, M. L., D. A. Lockner, and J. D. Byerlee, Frictional slip of granite at hydrothermal conditions, *J. Geophys. Res.*, *100*, 13,045–13,064, 1995.

Chester, F. M., and J. S. Chester, Ultracataclasite structure and friction processes of the Punchbowl fault, San Andreas system, California, *Tectonophysics*, *295*, 199–221, 1998.

Cocco, M., and A. Bizzarri, On the slip-weakening behavior of rate- and state-dependent constitutive laws, *Geophys. Res. Lett.*, *29*(11), 1516, doi:10.1029/2001GL013999, 2002.

Dieterich, J. H., and B. D. Kilgore, Direct observation of frictional contacts: New insights for state-dependent properties, *Pure Appl. Geophys.*, *143*, 283–302, 1994.

Dieterich, J. H., and B. D. Kilgore, Imaging surface contacts: power law contact distributions and contact stresses in quartz, calcite, glass and acrylic plastic, *Tectonophysics*, *256*, 219–239, 1996.

Dodge, D. A., G. C. Beroza, and W. L. Ellsworth, Detailed observations of California foreshock sequences: implications for the earthquake initiation process, *J. Geophys. Res.*, *101*, 22,371–22,392, 1996.

Ellsworth, W. L., and G. C. Beroza, Seismic evidence for an earthquake nucleation phase, *Science*, *268*, 851–855, 1995.

Ellsworth, W. L., F. Waldhauser, and A. Cole, A new view of the San Andreas Fault: Implications for earthquake interaction at Parkfield (extended abstract), Int. Sch. of Geophys., Erice, Sicily, 2000.

Fletcher, J. B., and P. A. Spudich, Rupture characteristics of three M ~ 4.7 (1992–1994) Parkfield earthquakes, *J. Geophys. Res.*, *103*, 835–854, 1998.

Ide, S., and M. Takeo, Determination of constitutive relations of fault slip based on seismic wave analysis, *J. Geophys. Res.*, *102*, 27,379–27,391, 1997.

Kilb, D., and J. Gomberg, The initial subevent of the 1994 Northridge, California, earthquake: Is earthquake size predictable?, *J. Seismol.*, *3*, 409–420, 1999.

Lapusta, N., Elastodynamic analyses of sliding with rate and state friction, Ph.D. thesis, Div. of Eng. and Appl. Sci., Harvard Univ., Cambridge, Mass., 2001.

Lapusta, N., J. R. Rice, Y. Ben-Zion, and G. Zheng, Elastodynamic analysis for slow tectonic loading with spontaneous rupture episodes on faults with rate- and state-dependent friction, *J. Geophys. Res.*, *105*, 23,765–23,789, 2000.

Lim, S. C., and M. F. Ashby, Wear mechanism maps, *Acta Metall*, *35*, 1–24, 1987.

Lim, S. C., M. F. Ashby, and J. H. Brunton, The effects of sliding conditions on the dry friction of metals, *Acta Metall.*, *37*, 767–772, 1989.

Marone, C., Laboratory-derived friction laws and their application to seismic faulting, *Annu. Rev. Earth Planet. Sci.*, *26*, 643–696, 1998.

Molinari, A., Y. Estrin, and S. Mercier, Dependence of the coefficient of friction on sliding conditions in the high velocity range, *J. Tribol.*, *121*, 35–41, 1999.

Mori, J., and H. Kanamori, Initial rupture of earthquakes in the 1995 Ridgecrest, California sequence, *Geophys. Res. Lett.*, *23*, 2340–2437, 1996.

Ohnaka, M., Critical size of the nucleation zone of earthquake rupture interred from immediate foreshock activity, *J. Phys. Earth*, *41*, 45–56, 1993.

Ohnaka, M., A physical scaling relation between the size of an earthquake and its nucleation zone size, *Pure Appl. Geophys.*, *157*(11–12), 2259–2282, 2000.

Olsen, K. B., R. Madariaga, and R. J. Archuleta, Three-dimensional dynamic simulation of the 1992 Landers earthquake, *Science*, *278*, 834–838, 1997.

Oppenheimer, D. H., W. H. Bakun, and A. G. Lindh, Slip partitioning of the Calaveras fault, California, and prospects for future earthquakes, *J. Geophys. Res.*, *95*, 8483–8498, 1990.

Poliakov, A. N. B., R. Dmowska, and J. R. Rice, Dynamic shear rupture interactions with fault bends and off-axis secondary faulting, *J. Geophys. Res.*, *107*(B11), 2295, doi:10.1029/2001JB000572, 2002.

Rice, J. R., Fault stress states, pore pressure distributions, and the weakness of the San Andreas fault, in *Fault Mechanics and Transport Properties of Rocks*, edited by B. Evans and T.-F. Wong, pp. 475–503, Academic, San Diego, Calif., 1992.

Rice, J. R., Spatio-temporal complexity of slip on a fault, *J. Geophys. Res.*, *98*, 9885–9907, 1993.

Rice, J. R., Flash heating at asperity contacts and rate-dependent friction (abstract), *Eos Trans. AGU*, *80*(46), Fall Meet. Suppl., F681, 1999.

Rice, J. R., and Y. Ben-Zion, Slip complexity in earthquake fault models, *Proc. Natl. Acad. Sci. U. S. A.*, *93*, 3811–3818, 1996.

Rice, J. R., and A. L. Ruina, Stability of steady frictional slipping, *J. Appl. Mech.*, *50*, 343–349, 1983.

Rice, J. R., N. Lapusta, and K. Ranjith, Rate and state dependent friction and the stability of sliding between elastically deformable solids, *J. Mech. Phys. Solids*, *49*, 1865–1898, 2001.

Schaff, D. P., G. H. R. Bokelmann, G. C. Beroza, F. Waldhauser, and W. L. Ellsworth, High-resolution image of Calaveras Fault seismicity, *J. Geophys. Res.*, *107*(B9), 2186, doi:10.1029/2001JB000633, 2002.

Stirling, M. W., S. G. Wesnousky, and K. Shimazaki, Fault trace complexity, cumulative slip, and the shape of the magnitude-frequency distribution for strike-slip faults; a global survey, *Geophys. J. Int.*, *24*, 833–868, 1996.

Tse, S. T., and J. R. Rice, Crustal earthquake instability in relation to the depth variation of frictional slip properties, *J. Geophys. Res.*, *91*, 9452–9472, 1986.

Tsutsumi, A., and T. Shimamoto, High-velocity frictional properties of gabbro, *Geophys. Res. Lett.*, *24*, 699–702, 1997.

Uenishi, K., and J. R. Rice, Universal nucleation length for slip-weakening rupture instability under nonuniform fault loading, *J. Geophys. Res.*, *108*(B1), 2042, doi:10.1029/2001JB001681, 2003.

Wesnousky, S., Seismicity as a function of cumulative geologic offset: Some observations from southern California, *Bull. Seismol. Soc. Am.*, *80*, 1374–1381, 1990.

Wesnousky, S. G., The Gutenberg-Richter or characteristic earthquake distribution, which is it?, *Bull. Seismol. Soc. Am.*, *84*, 1940–1959, 1994.

N. Lapusta, Division of Engineering and Applied Science, California Institute of Technology, Pasadena, CA 91125, USA. (lapusta@caltech.edu)

J. R. Rice, Division of Engineering and Applied Sciences, Harvard University, Cambridge, MA 02138, USA. (rice@esag.harvard.edu)